Strain relaxation in InGaN/GaN micro-pillars evidenced by high resolution cathodoluminescence hyperspectral imaging

E. Y. Xie, Z. Z. Chen, P. R. Edwards, Z. Gong, N. Y. Liu et al.

Related Articles

Photoluminescence of boron nitride nanosheets exfoliated by ball milling
Appl. Phys. Lett. 100, 261108 (2012)

Effect of proton bombardment on InAs dots and wetting layer in laser structures
Appl. Phys. Lett. 100, 261105 (2012)

Fabrication and luminescent properties of core-shell InGaN/GaN multiple quantum wells on GaN nanopillars
Appl. Phys. Lett. 100, 261103 (2012)

Exciton and carrier spin relaxations in InGaAs lattice-matched to off-cut Ge substrates
Appl. Phys. Lett. 100, 252414 (2012)

Controlled optical properties of GaSb/InGaAs type-II quantum dots grown on InP substrate
Appl. Phys. Lett. 100, 251908 (2012)

Additional information on J. Appl. Phys.

Journal Homepage: http://jap.aip.org/

Journal Information: http://jap.aip.org/about/about_the_journal

Top downloads: http://jap.aip.org/features/most_downloaded

Information for Authors: http://jap.aip.org/authors

Strain relaxation in InGaN/GaN micro-pillars evidenced by high resolution cathodoluminescence hyperspectral imaging

E. Y. Xie,[1] Z. Z. Chen,[1,2,a)] P. R. Edwards,[3] Z. Gong,[1] N. Y. Liu,[1,2] Y. B. Tao,[1,2] Y. F. Zhang,[1] Y. J. Chen,[1] I. M. Watson,[1] E. Gu,[1,a)] R. W. Martin,[3] G. Y. Zhang,[2] and M. D. Dawson[1]

[1]*Institute of Photonics, SUPA, University of Strathclyde, Glasgow G4 0NW, United Kingdom*
[2]*State Key Laboratory of Artificial Microstructure and Mesoscopic Physics, School of Physics, Peking University, Beijing 100871, China*
[3]*Department of Physics, SUPA, University of Strathclyde, Glasgow G4 0NG, United Kingdom*

A size-dependent strain relaxation and its effects on the optical properties of InGaN/GaN multiple quantum wells (QWs) in micro-pillars have been investigated through a combination of high spatial resolution cathodoluminescence (CL) hyperspectral imaging and numerical modeling. The pillars have diameters (d) ranging from 2 to 150 μm and were fabricated from a III-nitride light-emitting diode (LED) structure optimized for yellow-green emission at $\sim$560 nm. The CL mapping enables us to investigate strain relaxation in these pillars on a sub-micron scale and to confirm for the first time that a narrow ($\leq$2 μm) edge blue-shift occurs even for the large InGaN/GaN pillars (d > 10 μm). The observed maximum blue-shift at the pillar edge exceeds 7 nm with respect to the pillar centre for the pillars with diameters in the 2–16 μm range. For the smallest pillar (d = 2 μm), the total blue-shift at the edge is 17.5 nm including an 8.2 nm "global" blue-shift at the pillar centre in comparison with the unetched wafer. By using a finite element method with a boundary condition taking account of a strained GaN buffer layer which was neglected in previous simulation works, the strain distribution in the QWs of these pillars was simulated as a function of pillar diameter. The blue-shift in the QWs emission wavelength was then calculated from the strain-dependent changes in piezoelectric field, and the consequent modification of transition energy in the QWs. The simulation and experimental results agree well, confirming the necessity for considering the strained buffer layer in the strain simulation. These results **provide** not only significant **insights into the mechanism** of strain relaxation in these micro-pillars but also practical **guidance** for design of micro/nano LEDs. © *2012 American Institute of Physics*. [http://dx.doi.org/10.1063/1.4733335]

I. INTRODUCTION

III-nitride semiconductors, grown as epitaxial multi-layers with the wurtzite crystal structure, have enabled major recent advances in the technology of light-emitting diodes (LEDs). A particular driving force for LED technology is its applications in full-color displays and high-efficiency lighting. In the visible spectrum, InGaN-based quantum wells (QWs) form the active regions of nitride LEDs. External quantum efficiencies as high as $\sim$75% have been reported in state-of-the-art blue LED devices.[1] However, achieving high quantum efficiencies becomes an increasing challenge at longer wavelengths.[2] A critical factor for QWs grown in the conventional polar (0001) orientation is the pseudomorphic strain, and resulting large piezoelectric field, caused by the 11% difference in in-plane lattice parameters between GaN and InN. This piezoelectric contribution to the polarization field generates a larger quantum confined Stark effect (QCSE) as the InN fraction in the QWs increases. Consequently, for nitride LEDs emitting in the green-red visible, there is a progressive tendency for quantum efficiency to decrease as the emission wavelength increases.

The strain giving rise to the QCSE may be fully or partly relaxed in micro- or nano-scale GaN pillars, motivating a number of previous luminescence-based studies on such samples, usually focusing on photoluminescence results.[3–12] The fabrication method has typically involved "top-down" patterning by etching an initially planar epitaxial structure containing InGaN/GaN QWs, although studies of directly grown nano-columnar structures have also been reported.[12] Correlations between spectroscopic results and numerical simulations of strain relaxation in the QWs were included in the reports by Yu *et al.*[9] and Kawakami *et al.*[10] The authors of Ref. 9 employed an atomistic valence force field (VFF) method for strain calculations. Meanwhile in Ref. 10, the finite element method (FEM), embodying macroscopic elastic theory, was used. Analogous FEM calculations have proved effective in simulating semiconductor nanostructures including self-organized GaN/AlN quantum dots,[13] InAs quantum dots[14] and nanocolumnar GaN/AlGaN disks.[15] However, in choosing boundary conditions, previous authors have usually just considered the local environment of the QWs while neglecting the influence from other layers.[9,10,13,15] This assumption becomes increasingly inaccurate when the fill factor of etched mesas (the ratio of mesa area to total sample area) is very small and the height of the mesa is relatively large. Moreover, the spatial resolution of the photoluminescence measurements used so far was limited by the size of the beam spot. To the best of our knowledge, the highest resolutions achieved were 500 nm at room temperature and

a)Electronic addresses: z.z.chen@pku.edu.cn and erdan.gu@strath.ac.uk.

800 nm at 4.2 K.[10] With such resolutions, it is not possible to investigate the detailed strain relaxation process at a sub-micron scale and direct comparison between the experimental and simulation results is also hard to achieve. Clearly, further improvement of spatial resolution and simulation accuracy will enable a much better understanding of the ***mechanism*** of strain relaxation in the micro-GaN pillars, which is critically important to the design of novel micro/nano pixellated LED devices for a ***wide range of applications***.[4,16–19]

This study focuses on the strain relaxation process in micro-pillars fabricated from an LED wafer optimized for emission at yellow-green wavelengths (∼560 nm). These micro-pillars had a fixed height of 1.1 μm, and diameters systematically varied from 2 to 150 μm. High spatial resolution cathodoluminescence (CL) hyperspectral imaging[20,21] was used to record spectrally resolved emission from the pillars on a length scale of approximately 100 nm. The main phenomenon observed was the significant blue-shift in emission wavelength and its detailed distribution caused by strain relaxation in the QWs. For any individual micro-pillar, this blue-shift increased with proximity to the mesa edge, reaching a maximum value of ∼9 nm for the smallest pillar. The FEM method, explicitly including the GaN buffer layer and substrate below the emissive QWs, was used to calculate the strain distributions in these pillars as a function of mesa diameter. This information was in turn used to calculate the blue-shift in the QWs emission.

II. EXPERIMENTAL DETAILS

The InGaN/GaN LED wafer was grown on c-plane sapphire by metalorganic chemical vapor deposition. The epitaxial structure is illustrated in Fig. 1(a), and comprised the following functional layers: a 2 μm thick undoped GaN buffer layer; a 2 μm thick n-type GaN layer; two $In_{0.10}Ga_{0.90}N$ QWs of 3 nm thickness with 10 nm GaN barrier layers; six $In_{0.25}Ga_{0.75}N$ QWs again of 3 nm thickness and separated by 10 nm GaN barriers; and finally a 240 nm Mg-doped GaN layer. The first two QWs function as an electron reservoir layer (ERL) for improving the carrier capture rate[22] and mitigating the efficiency droop by reducing the overflow of "hot electrons".[23] In the context of this study, their presence also gave an opportunity to compare the effect of strain relaxation on QWs of different alloy compositions. The micro-pillars were fabricated with diameters ranging from 2 to 150 μm in a configuration described previously.[24] The top p-GaN layer was firstly thinned down to 40 nm by inductively coupled plasma (ICP) etching. This step facilitated CL measurements with high lateral resolution by reducing the accelerating voltages needed to excite QW emission. A 300 nm thick silicon dioxide (SiO_2) layer was then deposited on the p-GaN by plasma-enhanced chemical vapor deposition. The SiO_2 layer was then patterned into an array of micro-disks using photolithography followed by reactive ion etching. Defined by the SiO_2 mask, ICP etching was used to fabricate micro-pillars with a height of 1.1 μm which is typical for a LED fabrication process. Prior to the CL measurements, the SiO_2 mask was removed using a buffered hydrofluoric acid solution.
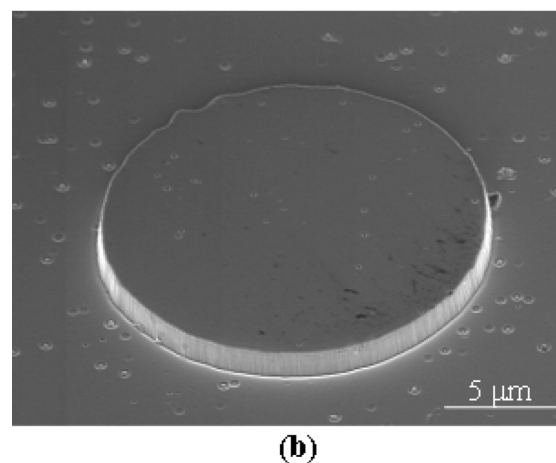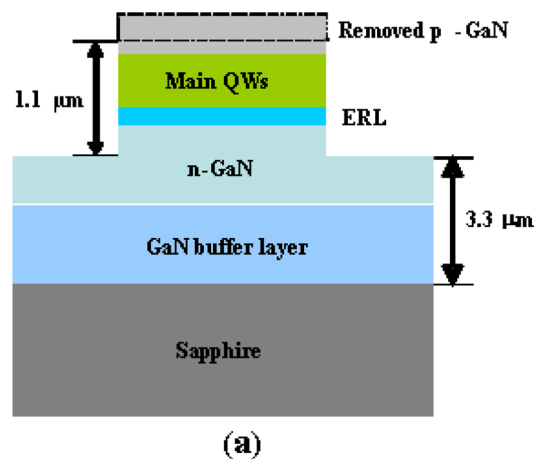

FIG. 1. (a) Schematic sequence of functional layers in the LED epiwafers, also showing the p-GaN layer removed to facilitate CL measurements and (b) oblique-view SEM image of an InGaN/GaN micro-pillar with diameter of 16 μm.

Room-temperature CL measurements were made using a custom-built detection system installed on an FEI Sirion 200 ultrahigh-resolution Schottky field-emission scanning electron microscope (SEM). The sample was inclined at 45° with respect to the electron beam and the luminescence was collected by a Schwarzschild-type reflecting objective at a right angle to the electron beam. The light was then coupled directly to the entrance slit of a 1/8 m spectrograph using a paraboloidal mirror and detected using a cooled electron-multiplying charge coupled device (EMCCD) detector.[21] An accelerating voltage of 5 kV and an electron beam current of 1.5 nA were used to limit the beam interaction volume (and hence spatial resolution) to ∼100 nm. A full CL spectrum was recorded at each point under a scanning beam, allowing CL spectra and maps to be later extracted from the resultant data cube. A significant advantage of this form of CL measurement over the conventional methods of monochromatic imaging or fixed-point spectroscopy is that it allows shifts in emission wavelength to be mapped.[25] This advanced capability is indispensable for investigating the strain distributions in the micro-GaN/InGaN pillars.

The strain distributions in the micro-pillars were also simulated using the ANSYS 11.0 commercial finite element software package. In order to include the influences between

TABLE I. Parameters used for different materials in the FEM simulations. The lattice constants and elastic constants for GaN and InN are cited from Ref. 28.

Materials	C_{11} (GPa)	C_{12} (GPa)	C_{13} (GPa)	C_{33} (GPa)	C_{44} (GPa)	a (Å)
GaN	390	145	106	398	105	3.189
Sapphire	490	165.4	113	490	145.4	4.758
$In_{0.1}Ga_{0.9}N$	373.3	142	104.6	380.6	99.3	3.225
$In_{0.25}Ga_{0.75}N$	348.3	137.5	102.5	354.5	90.75	3.278

neighboring pillars, simulations were performed on 5×1 arrays of identically sized pillars. These arrays had a pitch chosen to give a fill factor of 26%, corresponding to the average value for the repeating unit in the arrays of fabricated pillars.[24] The strain distribution calculated for the middle pillar was used to estimate the spectral shifts. The in-plane strain isotropy for the (0001) growth orientation allowed the simulation to be simplified to a two-dimensional case. All the III-nitride layers shown in Fig. 1(a) were included in the simulation, although the FEM model did not extend through the full thickness of the sapphire substrate. Detailed analysis of the wafer bowing predicts that a bending-free plane is at a depth of $\sim$70 μm;[26] we therefore included 80 μm thick sapphire in order to define a practical boundary condition. Pillar sidewalls were left free from constraints. A strain variation with epilayer thickness as shown in Ref. 27 was used for estimating the residual strain in the GaN buffer layer below the first ERL QW, which will be discussed in the next part in more detail, while pseudomorphic growth was assumed for all QWs. Based on the data from Ref. 28 and Vegard's law (linear interpolation), unstrained lattice parameters and elastic constants were calculated for the two relevant $In_xGa_{1-x}N$ compositions. These calculated values are summarized in Table I. Actual strain simulations for the $In_xGa_{1-x}N$ QWs were performed by a thermoelastic method accommodated within ANSYS.[13,14] The piezoelectric polarization tensor was then calculated by the "E-first" route preferred by Christmas *et al.*[29] Finally, by introducing the piezoelectric potential into the one–dimensional Schrödinger equation, and neglecting the inbuilt p-n junction field and carrier screening effects, the optical transition energy of the QW was calculated with MATLAB software. In later discussion, the calculated transition energies are compared with the measured QW emission energies directly, i.e., the Stokes shift was assumed to be constant. In this work, as the pillar sizes are in micro-scale, the alteration of QW transition energies due to lateral quantum confinement, which was considered in certain nano-pillar structures,[7,9] can be neglected.

III. RESULTS AND DISCUSSIONS

Fig. 1(b) shows an SEM image of a representative InGaN/GaN micro-pillar, with a diameter of 16 μm. It can be seen that the top surface of the pillar is smooth, but shows occasional pits which are likely to have resulted from ICP etching around structural defects. The sidewall is almost perpendicular to the surrounding surface, with an inclination angle of about 85°. Fig. 2(a) shows typical CL spectra extracted from the centre and edge of this pillar,

corresponding to the areas marked by squares in Fig. 2(b). There are two emission peaks from the InGaN/GaN multiple-quantum-well (MQW) layers visible in the CL spectra, centered at 560 nm in the yellow-green and at 425 nm in the blue. The strong yellow-green emission originates from the $In_{0.25}Ga_{0.75}N$ QWs, which is also the dominant emission in the electroluminescence (EL) spectrum of a 16 μm micro-pillar LED (μ-LED) fabricated from the same epiwafer (without thinning down the top p-GaN layer so as to achieve good ohmic contact) as shown in the insert in Fig. 2(a). The blue luminescence in both CL and EL spectra is emitted from the $In_{0.10}Ga_{0.90}N$ ERL QWs. The EL spectrum of μ-LEDs at a low injection current of 1 mA (to exclude thermal effects during the LED operation) is similar to the CL emission. The main emission peak in EL shows a slightly greater blue-shift than that we observed at the edge of pillars. This may be due to the inhomogeneous indium distribution in such a high indium content wafer or the differences in the carrier screening and/or band filling effect between the two excitation methods. Another difference between the measured CL and EL spectra is the relatively weaker blue emission observed in EL. This may be due to the heavy effective mass and low mobility of holes in GaN which limit the migration distance of holes. In contrast, the penetration depth in CL measurements depends mainly on the acceleration voltage used rather than the diffusion/drift length of carriers which could result in a more pronounced CL signal from the ERL QWs. A detailed study of μ-LEDs fabricated by using the same wafer has been reported recently.[30]

Unlike the area-integrated spectra of EL, CL is highly spatially resolved, allowing high resolution hyperspectral imaging to be carried out. As shown in Fig. 2(a), the yellow-green emission from the edge (the black curve) shows a blue-shift in emission wavelength and intensity enhancement compared with that from the center (the red curve). There is no comparable spectral shift or intensity enhancement for the blue emission. The spectral shift and enhanced emission can be largely attributed to the reduction of the QCSE by partial strain relaxation. Figs. 2(b) and 2(c) show CL wavelength maps corresponding to the yellow-green QWs and blue ERL QWs emissions respectively from this 16 μm pillar. These maps were extracted from CL hyperspectral images with a scanning step size of 200 nm using nonlinear least-squares peak fitting. Fig. 2(b) shows a clear blue-shift ring around the pillar perimeter with a maximum shift value of $\sim$7 nm relative to the centre. However, Fig. 2(c) shows no corresponding blue-shift ring at the edge of the pillar in the ERL emission. To further illustrate the variation of emission wavelength, line-scans of the peak emission wavelengths in the two spectral regions are plotted along a typical diameter of the pillar as shown in Fig. 2(d). The longer wavelength data highlight the blue-shifts reaching 7 nm within the 2 μm region around the pillar edge. Wavelength fluctuations from the mean of $\sim$3 nm peak-to-peak are seen in the centre area of the pillar, and their non-systematic distribution suggests that such fluctuations are from variations in indium nitride fraction and/or other inhomogeneities in the yellow-green QWs. This degree of intrinsic variation was considered in choosing a threshold shift of 3 nm to define the blue-shifted
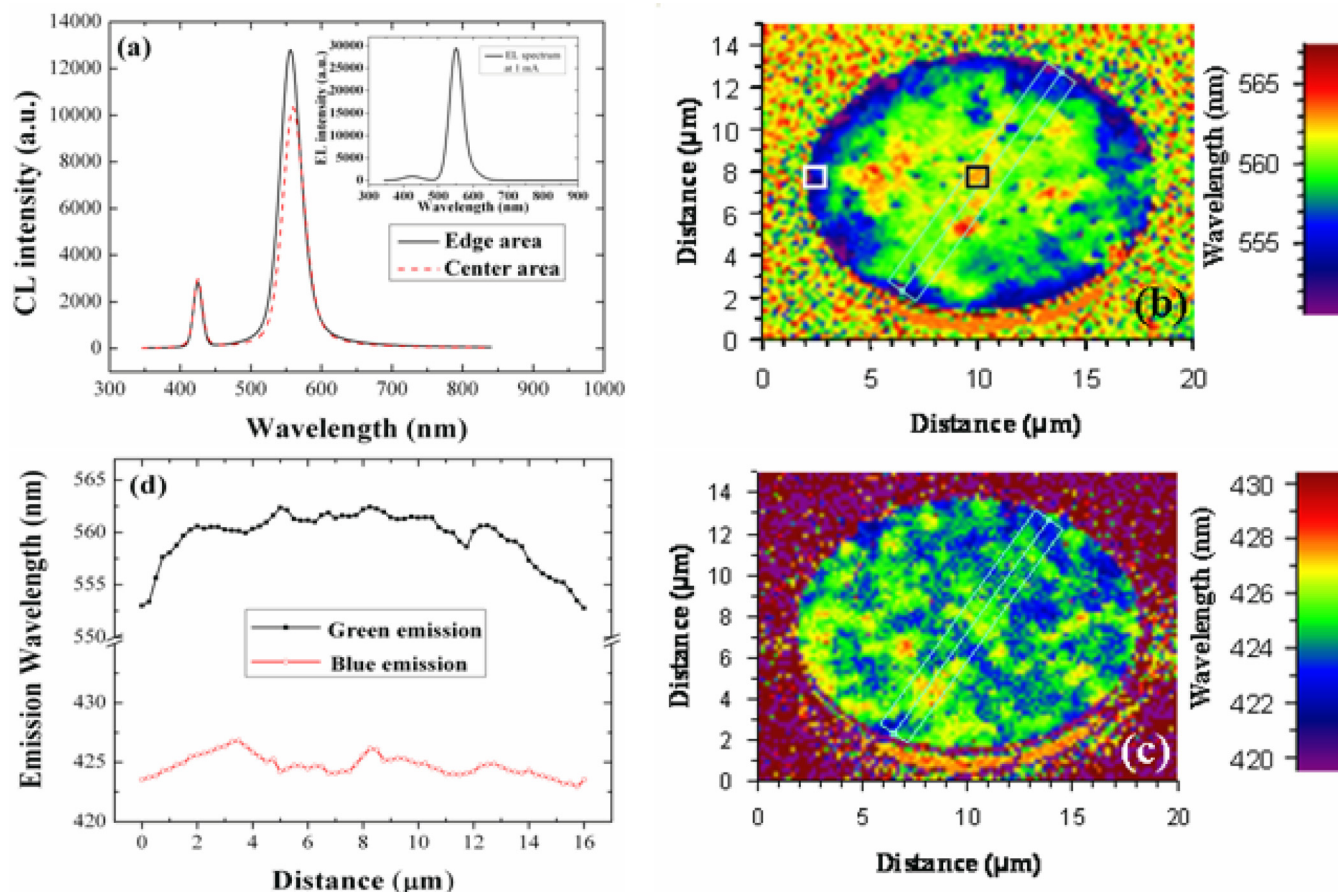
FIG. 2. Various presentations of the spatially resolved CL characteristics of a 16-μm pillar: (a) typical spectra recorded from edge and center areas as marked in part (b), the insert is the EL spectrum of a 16 μm μ-LED measured at an injection current of 1 mA; (b) wavelength map in the yellow-green spectral region; (c) wavelength map in the blue spectral region, corresponding to emission from the main QWs and ERL QWs; (d) variations of emission wavelength on along representative pillar diameters as shown in parts (b) and (c).

zone whose spatial extent is analyzed in later discussion. The line-scan data for the blue QW emission confirm that any systematic blue-shift towards the pillar edge is indistinguishable from the fluctuation and thus constrain any such shift to below 1–2 nm in magnitude.

It is notable that a blue-shift ring region of the yellow-green QW emission at the edge of the pillar appears even when the pillar diameter is larger than 10 μm. To the best of our knowledge, this is the first observation of such a blue-shift and its ring shape distribution in the large pillars, made possible by the high-resolution CL mapping technique. Our measurements also confirmed that the blue-shift in the blue QWs emission is too small to be observed due to the lower lattice mismatch between the active layers and barriers, which is consistent with our previous research.[4]

Fig. 3 shows the simulated in-plane compressive strain distribution (i.e., the ε_{xx}, a component of the strain tensor) at the edge of a pillar with a diameter of 16 μm. The colour-coded range of the in-plane strain as per the key in the figure has been set to highlight the strain variations in the six In$_{0.25}$Ga$_{0.75}$N/GaN QWs. The two underlying ERL QWs and the surrounding GaN are shown in gray, as the strain in these regions is outside the color-coded range (less compressive strain in low InN fraction QWs and tensile strain in GaN layers). The simulation reveals that ε_{xx} is reduced by up to

12.5% from -2.71×10^{-2} at the centre to -2.37×10^{-2} at the pillar edge for the In$_{0.25}$Ga$_{0.75}$N QWs. This change in strain corresponds to an average blue-shift in the transition wavelength of 7.4 nm, which agrees well with the experimental result shown in Fig. 2(d). The simulation also confirmed that the strain remains almost unchanged in the central 75% area of the pillar. Compared with the initial strain in the as-grown yellow-green QWs (-2.72×10^{-2}, which was calculated from stain-free lattice constants) caused by lattice mismatch, the maximum compressive strain in the pillar centre is also reduced, corresponding to a calculated global blue-shift of 1.3 nm. The calculated width of the blue-shifted ($\Delta\lambda > 3$ nm) region at the pillar edge is around 1 μm, which is slightly smaller than the average result observed by CL mapping. This may be due to the uncertain residual strain induced in the GaN buffer layer and will be discussed later. For the two lower ERL In$_{0.1}$Ga$_{0.9}$N QWs (not colored in Fig. 3), similar phenomena are observed. The in-plane strain is reduced up to 16.5% at the pillar edge and the maximum strain at the pillar centre is also slightly relaxed by the micro-patterning. However, the corresponding blue-shift of ERL QWs emission is less than 2 nm on average, which is hardly resolvable against the background fluctuation in CL maps. Therefore, we will mainly focus on the strain relaxation in high indium content QWs.
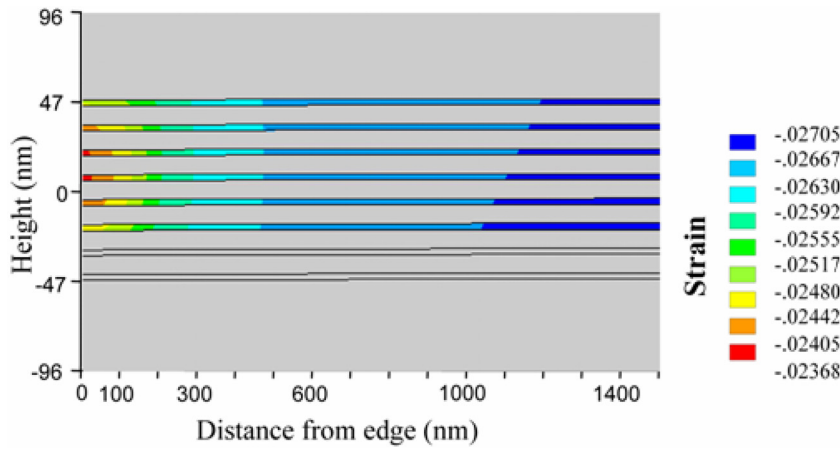
FIG. 3. The simulated in-plane strain (ε_{xx}) distribution at the edge of an InGaN/GaN MQW micro-pillar with a diameter of 16 μm.

In addition to the 16 μm pillar, CL measurements and simulations were also extended to a series of pillars with diameters from 2 to 150 μm. The black data points in Fig. 4 show the trends observed in maximum blue-shift at the pillar edge relative to the pillar centre [Fig. 4(a)], the width of the blue-shift ring region (defined by $\Delta\lambda > 3$ nm, as above) [Fig. 4(b)], the ratio of this blue-shift ring region to the whole pillar area [Fig. 4(c)], and the global blue-shift observed at the pillar centre relative to non-patterned epiwafer [Fig. 4(d)] as a function of pillar diameter for the yellow-green QWs. The red data points show corresponding simulation results. All measured data points plotted in Fig. 4 were derived by averaging 10 line-scans across a pillar diameter, as previously illustrated in Fig. 2(d). As shown in Fig. 4(a), the magnitude of the measured maximum shift decreases from 9.3 nm to 5.6 nm as the pillar diameters increases from 2 to 150 μm, becoming almost constant (around 6 nm) for pillar diameters in excess of 30 μm. In Fig. 4(b), the width of the $\Delta\lambda > 3$ nm blue-shift ring region at the pillar edge
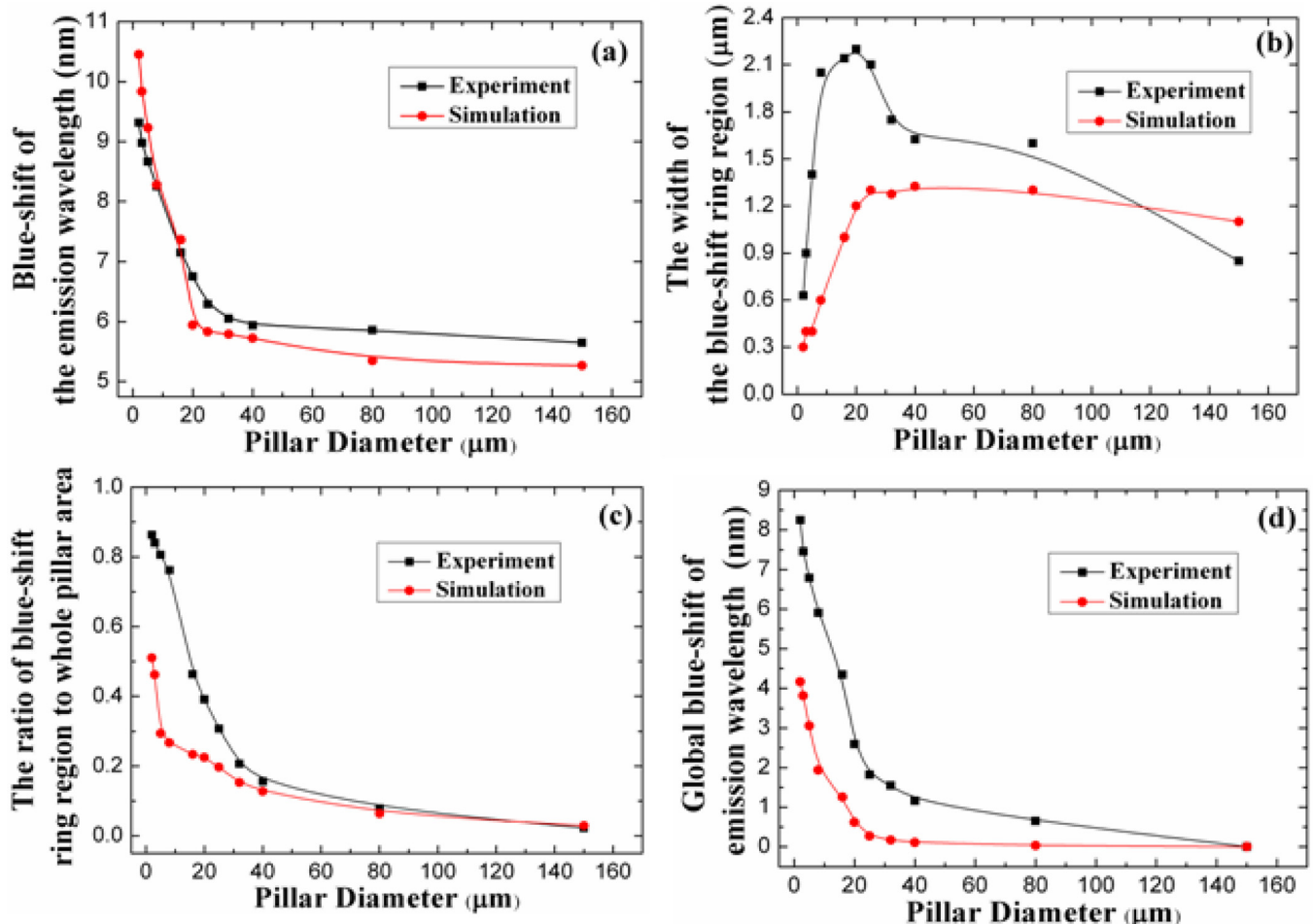

FIG. 4. Experimental and simulated values for spectral shift parameters as a function of pillar diameter: (a) the maximum blue-shift of the emission wavelength at the pillar edge relative to pillar centre; (b) the width of the blue-shift ring region; (c) the ratio of the blue-shift ring region to whole pillar area; and (d) the global blue-shift of the emission wavelength at the pillar centre. All lines are guides to the eye.

is observed to reach a maximum value of ~2.2 μm for a 20 μm pillar. However, as shown in Fig. 4(c), the proportion of this area decreases continuously as the pillar diameter increases, from 86% at 2 μm to only 3% at 150 μm. These results confirmed that for the smaller micro-pillars studied, the majority of the volume is significantly strain relaxed, and there is a strong gradient in the strain relaxation towards the edge. Fig. 4(d) shows the global blue-shift of the emission wavelength, meaning the blue-shift at the pillar centre relative to the as-grown epiwafer. This global blue-shift decreases with increasing pillar diameter, starting from a value of 8.2 nm for the 2 μm pillar. It can be seen that over 30 μm, the decrease of this global blue-shift of emission wavelength becomes slow and a zero global blue-shift is observed for the largest (150 μm) pillar. Clearly, these CL measurements indicate that the strain relaxation becomes dominant when the pillar size is less than 30 μm. This information provides an important guideline for designing high efficiency micro-LEDs.

The red points in the Fig. 4 group show simulated values for the various parameters discussed above. For these simulations, the small contribution of strain dependent changes in Stokes shift was not considered.[6,31] Clearly, the trends of the experimental and simulated results are nearly the same. In Fig. 4(a), the maximum blue-shift values measured agree very well with the simulation results for the smaller pillars, while only a slight difference is observed when the pillar diameter is larger than 16 μm. This suggests that our data collection and processing methods aimed at achieving high lateral resolution have successfully met the challenges of wavelength shift measurements on the smaller pillars imposed by intrinsic QW inhomogeneities and the strain gradients close to the pillar sidewalls. Nevertheless, as shown in Fig. 4, some differences between the measured and simulated values were observed. A possible explanation for these differences is that the fill factors are slightly different for the fabricated micro-pillar arrays and for the simulation model. The fit for the smaller pillars would be improved by performing the simulations with smaller fill factors, which would give larger global strain relaxations and wider blue-shifted regions. Another relevant factor is the strain value assumed in the GaN buffer layer immediately below the first ERL QW. The in-plane compressive strain used in our simulation was 1.34×10^{-3}, which was interpolated from the experimental value reported in Ref. 27. Although this strain is one order smaller than the ones in the QWs, it significantly influences the strain transfer and distribution in the whole wafer, which has been confirmed by repeating the simulation with a series of different assumed strain values. While not increasing the magnitude of the blue-shift at the edge of the pillar, lowering the strain in the buffer GaN widens the blue-shift area and increases the global blue-shift of the pillars, giving better agreement with our experimental CL results.

Compared with the previous relevant studies,[9,10] our work demonstrates that the strain relaxation in these micro-pillars is strongly location dependent. The strain relaxations at the pillar centre and edge are dramatically different, resulting in two blue-shifts, i.e., the maximum blue-shift at the pillar edge and the global blue-shift at the pillar centre as illustrated in Figs. 4(a) and 4(d). For a 2 μm pillar, the blue-shift at the pillar edge is as high as 17.5 nm relative to a non-patterned epiwafer. This value agrees well with the results shown in Ref. 10. Furthermore, compared with the previous fluorescence microscope images, our high resolution CL hyperspectral imaging reveals a much more detailed emission wavelength distribution in these micro-pillars and thus enables us to investigate the local strain relaxations. Our detailed analysis of CL maps shows there is a broad ring shape strain relaxation region at the pillar edge of all the pillars investigated. This ring shape region had previously only been observed in smaller (<2 μm) pillars.[10] It is considered that the pillar's overall PL and/or EL spectrum is determined by the ratio of this ring region to the whole pillar area.

Additionally, in our simulation model, the strains in the areas outside micro-pillars were considered. We also took account of not only the strain induced from lattice mismatch in the active region but also the residual strain in GaN buffer layer. Furthermore, in the model, both compressive strain in QWs and whole wafer bending were considered at the same time. By these improvements, the calculated blue-shifts agreed well with the values obtained by CL measurements.

IV. CONCLUSIONS

In summary, the high resolution CL hyperspectral imaging technique has been used to investigate the strain relaxation in InGaN/GaN MQW micro-pillars with diameters ranging from 2 to 150 μm. The epitaxial MQW material studied was optimized for fabricating LEDs emitting in the yellow-green and included electron reservoir layers. These CL maps measured the detailed distributions in the QW emission wavelength attributable to changes in strain, as well as to intrinsic QW inhomogeneities. Peak emission wavelengths as a function of position have been calculated using finite element strain simulations and solution of the Schrödinger equation with appropriately chosen piezoelectric fields. The significant blue-shifts observed at the edge of the pillars are due to the partial relaxation of compressive strain in the QWs. This blue-shift and its ring shape distribution could be observed even when the pillar diameter is larger than 30 μm. With decreasing pillar size, the maximum blue-shift at the pillar edge and the ratio of this maximum blue-shift region to the whole pillar area, are both increased. Moreover, a significant global blue-shift persisting to the pillar centre is also observed for the small pillars. Simulated spectral shifts agree well with the experimental CL results when the strained nature of the GaN buffer layer is taken account. No previous studies, to our knowledge, have reported the comparisons between simulated spectral shifts and experimental measurements for such a wide range of pillar diameters. The results of this study are directly relevant to the further technological development of micro/nano-LED array devices, in particular predicting significant effects from strain relaxation for LED diameters below ~30 μm.

ACKNOWLEDGMENTS

[1] Y. Narukawa, M. Sano, M. Ichikawa, S. Minato, T. Sakamoto, T. Yamada, and T. Mukai, Jpn. J. Appl. Phys. Part 2 **46**, L963 (2007).

[2] M. H. Crawford, IEEE J. Sel. Top. Quantum Electron **15**, 1028 (2009).

[3] L. Dai, B. Zhang, J. Y. Lin, and H. X. Jiang, J. Appl. Phys. **89**, 4951 (2001).

[4] H. W. Choi, C. W. Jeon, M. D. Dawson, P. R. Edwards, R. W. Martin, and S. Tripathy, J. Appl. Phys. **93**, 5978 (2003).

[5] T.-H. Hseuh, H.-W. Huang, C.-C. Kao, Y.-H. Chang, M.-C. Ou-Yang, H.-C. Kuo, and S.-C. Wang, Jpn. J. Appl. Phys. **44**, 2661 (2005).

[6] S. Keller, C. Schaake, N. A. Fichtenbaum, C. J. Neufeld, Y. Wu, K. McGroddy, A. David, S. P. DenBaars, C. Weisbuch, J. S. Speck, and U. K. Mishra, J. Appl. Phys. **100**, 054314 (2006).

[7] H. S. Chen, D. M. Yeh, Y. C. Lu, C. Y. Chen, C. F. Huang, T. Yi. Tang, C. C. Yang, C. S. Wu, and C. D. Chen, Nanotechnology **17**, 1454 (2006).

[8] H. J. Chang, Y. P. Hsieh, T. T. Chen, Y. F. Chena, and C. T. Liang, Opt. Express **15**, 9357 (2007).

[9] P. C. Yu, C. H. Chiu, Y. R. Wu, H. H. Yen, J. R. Chen, C. C. Kao, H. W. Yang, H. C. Kuo, T. C. Lu, W. Y. Yeh, and S. C. Wang, Appl. Phys. Lett. **93**, 081110 (2008).

[10] Y. Kawakami, A. Kaneta, L. Su, Y. Zhu, K. Okamoto, M. Funato, A. Kikuchi, and K. Kishino, J. Appl. Phys. **107**, 023522 (2010).

[11] V. Ramesh, A.Kikuchi, K. Kishino, M. Funato, and Y. Kawakami, J. Appl. Phys. **107**, 114303 (2010).

[12] Y. Kawakami, S. Suzuki, A. Kaneta, and M. Funato, A. Kikuchi, and K. Kishino, Appl. Phys. Lett. **89**, 163124 (2006).

[13] Y. M. Liu, Z. Y. Yu, X. M. Ren, and Z. H. Xu, Chin. Phys. B **17**, 3471 (2008).

[14] T. Benabbas, P. Francois, Y. Androussi, and A. Lefebvre, J. Appl. Phys. **80**, 2764 (1996).

[15] J. Ristić, C. Rivera, E. Calleja, S. Fernández-Garrido, M. Povoloskyi, and A. Di Carlo, Phys. Rev. B **72**, 085330 (2005).

[16] H. X. Jiang, S. X. Jin, J. Li, J. Shakya, and J. Y. Lin, Appl. Phys. Lett. **78**, 1303 (2001).

[17] H. W. Choi, C. W. Jeon, and M. D. Dawson, IEEE Electron. Dev. Lett., **25**, 277 (2004).

[18] Z. Gong, H. X. Zhang, E. Gu, C. Griffin, M. D. Dawson, V. Poher, G. Kennedy, P. M. W. French, and M. A. A. Neil, IEEE Trans. Electron. Dev. **54**, 2650 (2007).

[19] Z. Liu, K. M. Wong, C. W. Keung, C. W. Tang, and K. M. Lau, IEEE J. Sel. Top. Quantum Electron. **15**, 1298 (2009).

[20] R. W. Martin, P. R. Edwards, K. P. O'Donnell, M. D. Dawson, C. W. Jeon, C. Liu, G. R. Rice, and I. M. Watson, Phys. Status Solidi A **201**, 665 (2004).

[21] P. R. Edwards and R. W. Martin, Semicond. Sci. Technol. **26** 064005 (2011).

[22] N. Otsuji, K. Fujiwara, and J. K. Sheu, J. Appl. Phys. **100**, 113105 (2006).

[23] X. Ni, X. Li, J. Lee, S. Liu, V. Avrutin, Ü. Özgür, H. Morkoç, A. Matulionis, T. Paskova, G. Mulholland, and K. R. Evans, Appl. Phys. Lett. **97**, 031110 (2010).

[24] Z. Gong, S. R. Jin, Y. J. Chen, J. McKendry, D. Massoubre, I. M. Watson, E. D. Gu, and M. D. Dawson, J. Appl. Phys. **107**, 013103 (2010).

[25] P. R. Edwards, R. W. Martin, I. M. Watson, C. Liu, R. A. Taylor, J. H. Rice, J. H. Na, J. W. Robinson, and J. D. Smith, Appl. Phys. Lett. **85**, 4281 (2004).

[26] Y. Jang, W. R. Kim, D.-H. Jang, J.-I. Shim, and D.-S. Shin, J. Appl. Phys. **107**, 113537 (2010).

[27] D.C. Reynolds, D.C. Look, B. Jogai, J. E. Hoelscher, R. E. Sherriff, and R. J. Molnar, J. Appl. Phys. **88**, 1460 (2000).

[28] I. Vurgaftmann, and J. R. Meyer, J. Appl. Phys. **94**, 3675 (2003).

[29] U. M. E. Christmas, A. D. Andreev, and D. A. Faux, J. Appl. Phys. **98**, 073522 (2005).

[30] Z. Gong, N. Y. Liu, Y. B. Tao, D. Massoubre, E. Y. Xie, X. D. Hu, Z. Z. Chen, G. Y. Zhang, Y. B. Pan, M. S. Hao, I. M. Watson, E. Gu, and M. D. Dawson, Semicond. Sci. Technol. **27**, 015003 (2012).

[31] R. W. Martin, P. G. Middleton, K. P. O'Donnell, and W. Van der Stricht, Appl. Phys. Lett. **74**, 263 (1999).